Models of stationary siphon flows in stratified, thermally conducting coronal loops: II - Shocked Solutions

S. Orlando[1], G. Peres[1] and S. Serio[1,2]
[1] Istituto ed Osservatorio Astronomico,
Piazza del Parlamento 1, 90134 Palermo, Italy
[2] IAIF, CNR Palermo, Italy
E-mail: orlando@oapa.astropa.unipa.it, peres@oapa.astropa.unipa.it,
serio@oapa.astropa.unipa.it

Abstract

We use a detailed hydrodynamic model which takes into account the effects of gravity, of radiative losses, of thermal conduction and of a parametrized heating term to explore the conditions for the presence of stationary shocks in critical and supersonic siphon flows in coronal loops. We consider separately isothermal and adiabatic shocks. The exploration of the parameter space shows that in every solution, as characterized by loop length, base dynamical pressure and base velocity, the shock position depends on the volumetric heating rate of the loop. In addition, with the exception of the critical solutions with isothermal shocks, there exists a range of volumetric heating rates for which there are two alternative positions where the shock can form. Scaling laws for supersonic solutions are derived.

Keywords. MHD - Sun: Chromosphere - Sun: Corona

1 Introduction

In a previous paper (Orlando, Peres & Serio 1994; hereafter Paper I), we have presented a detailed hydrodynamic model of stationary siphon flows in a semicircular solar coronal loop of constant cross section. The model was based on the equations of continuity, momentum, and energy conservation, taking into account the effect of gravity, the thermal conduction, the radiative losses from the optically thin coronal plasma and a uniform volumetric heating rate along the loop. We have explored thoroughly the space of solutions, and derived scaling laws for subsonic solutions which extend those of Rosner, Tucker and Vaiana (1978) and those of Serio et al. (1981) to the siphon flows. Such scaling laws relate the dynamic pressure $p+\rho v^2$, the maximum loop temperature, the loop semilength and the volumetric heating rate.

In Paper I we have also identified four classes of solutions: 1) subsonic solutions in which the Mach number, defined as $M = v/\sqrt{p/\rho}$, where v is the flow velocity, p the plasma pressure, and ρ the mass density of the plasma, is less than 1 along all the loop, 2) critical solutions in which, simultaneously, $M = 1$ and the divergence of velocity $\partial v/\partial s \neq 0$ at the critical point, 3) supersonic solutions with $M > 1$ along all the loop, and 4) unphysical solutions (mostly double-valued solutions). The critical solutions can be distinguished in two subclasses: solutions with monotonically increasing velocity (in the following called $y_<$) and solutions with monotonically decreasing velocity(in the following $y_>$). As we have discussed in Paper I, the characteristics of the solutions space can depend significantly on the boundary conditions: for instance, changing the heat flux at the base of the upflowing leg, the characteristics of solutions change and, among other things, the existence of supersonic solutions may not be allowed.

In this paper we analyze and discuss siphon flows subject to shocks inside coronal loops. As for critical solutions, the velocity increases monotonically, starting from the base of the upflowing leg, and becomes supersonic at the critical point. Since the plasma flow has to stop, eventually, on reaching the solar surface at the other end of the loop, the only way to match the two conditions is to assume a shock, somewhere in the descending branch, connecting the critical solution to a subsonic solution. One can also, in principle, imagine the existence of flows which start supersonic at the base of the loop, follow the supersonic branch of the solutions and are eventually decelerated, before reaching the solar surface, by a shock.

The characteristics of shocked supersonic solutions have not been studied at a deep level of detail, although potentially interesting for the phenomenology of the solar atmosphere (for instance for those observations of loops which hardly fit hydrostatic loop models, or which show part of the loop in broad band observations). Some attention to shocks in siphon flows has been paid by Cargill and Priest (1980), Noci (1981), Borrini and Noci (1982), Thomas (1988), Montesinos and Thomas (1989), Robb and Cally (1992), and, more recently and more in details by Degenhardt et al. (1993), whose work has been based, however, on a model which does not include thermal conduction, as the one we use.

With these considerations in mind, in the present paper we will extend our study of siphon flows in stratified, thermally conducting coronal loops to solutions with shocks, thoroughly studying their solutions space.

The paper is so structured: in Sect. 2 we briefly discuss the siphon flow model, in Sect. 3 we make some general considerations about shocks, in Sect. 4 we study the presence and the effects of shocks in critical and in supersonic solutions, and finally in Sect. 5 we draw our conclusions.

2 The siphon flow model

In our model of stationary siphon flows we assume a semicircular coronal loop of length $2L$ and uniform cross-sectional area which contains low β plasma. We take into account the effects of gravity, thermal conduction, radiative losses and volumetric heating rate which we consider uniform along the loop. The model equations are

$$\rho v = j \tag{1}$$

$$\rho v \frac{\partial v}{\partial s} = -\frac{\partial p}{\partial s} + \rho g \tag{2}$$

$$\frac{1}{2}\left(5p\frac{\partial v}{\partial s} + 3v\frac{\partial p}{\partial s}\right) - \frac{\partial}{\partial s}\left(\kappa\frac{\partial T}{\partial s}\right) = E_H - \frac{p^2}{4k_B^2T^2}\Lambda(T) \tag{3}$$

$$\rho = \mu m_H n, \quad \kappa = 9.2 \cdot 10^{-7} T^{5/2}, \tag{4}$$

$$g = -g_0 \cos\left(\frac{\pi s}{2L}\right), \quad p = 2nk_BT \tag{5}$$

where j, the mass flux, is constant, ρ is the mass density of plasma, v is the plasma velocity, s is the field lines coordinate, p is the pressure, g is the component of gravity parallel to the field lines, κ is the thermal conductivity given by Spitzer (1962), T is the temperature, E_H is the volumetric input power into the solar atmosphere, k_B is the Boltzmann constant, $\Lambda(T)$ is the radiative losses per unit emission measure (Raymond and Smith 1977), n is the hydrogen number density, $\mu = 1.257$ is the mean atomic mass for solar abundances, m_H is the mass of the hydrogen atom, g_0 is the solar surface gravity and L is the semilength of the loop.

The fluid equations are solved choosing the footpoint temperature to be $2 \cdot 10^4$ K and for different values of velocity, density and heat flux at the base of the upflowing leg.

In order to achieve high reliability close to critical points, we solve the fluid equations with two independent and refined codes: the first based on a fourth-order Runge-Kutta method with adaptive stepsize control and the second on a Bulirsch-Stoer method (Press et al. 1986, Stoer and Bulirsch 1980). Further details on the numerical techniques used in our codes are in Paper I.

3 Shock conditions

As mentioned in the Introduction, shocks will occur in siphon flows whenever a critical, or an entirely supersonic, flow has to match slow speed conditions at the base of the descending leg. As routinely done in, for instance, wind flow studies, the shock position is determined by the Rankine-Hugoniot (in the following RH) jump conditions for stationary shock transitions; the boundary conditions at the footpoints of the loop are equally important in such calculations. In the following we shall discuss some conditions governing the changes of the fluid variables across the shock.

Assuming that γ, the ratio of specific heats, is a constant, the RH conditions and the equation of state lead to

$$v_+ = \left(\gamma - 1 + \frac{2\gamma}{M_-^2}\right) \frac{v_-}{\gamma + 1} \,, \tag{6}$$

where v_- and v_+ are the pre-shock and post-shock velocity, respectively, and M_- is the Mach number before the shock (our notation in this work is based on the convention that the flow is supersonic before the shock). In appendix A, we report the details of the derivation.

A compression shock wave ($v_+ < v_-$) can occur for $M_-^2 > \gamma$, and a rarefaction wave ($v_+ > v_-$) can occur in the range $1 < M_-^2 < \gamma$. However rarefaction shock waves are impossible (see for example Zel'dovich & Raizer 1966), therefore we have to consider only the condition for the existence of a compression shock wave.

The forbidden range $1 < M_-^2 < \gamma$ reduces to a point for isothermal ($\gamma = 1$) shocks and in this case a compression shock wave can occur as long as $M_-^2 > 1$, i.e. as long as the flow is supersonic.

We shall now investigate the range of M_- in which the shock brings the velocity from a supersonic value to a subsonic value (i.e. $v_+ < c_+$, with c_+ the post-shock isothermal sound speed). Again, Eq. (6) and the condition $v_+ < c_+$ yield the condition

$$M_-^2 > \frac{3\gamma - 1}{3 - \gamma} \,. \tag{7}$$

Appendix B reports the detailed derivation of inequality (7). For isothermal shocks the condition reduces to $M_-^2 > 1$.

Therefore a compression shock wave with supersonic post-shock velocity exists in the range $\gamma < M_-^2 < (3\gamma - 1)/(3 - \gamma)$; and a compression shock wave with subsonic post-shock velocity exists for $M_-^2 > (3\gamma - 1)/(3 - \gamma)$. For the isothermal case ($\gamma = 1$) only a compression shock wave with subsonic post-shock velocity can exist.

4 Results

In our simulations, since we want solutions matching very low chromospheric downflow velocity, we consider only the compression shock wave with subsonic post-shock velocity discussed above. In this section we analyze stationary shocks in the solutions having a supersonic branch, i.e. the critical and the supersonic solutions. We discuss two extreme cases: isothermal shocks ($\gamma = 1$) and adiabatic shocks ($\gamma = 5/3$). All the other kinds of shocks fall in between these two.

4.1 Shocks in critical solutions

We have analyzed the class of the shocked critical solutions for a set of coronal loop models covering a grid of conditions, namely base dynamical pressure $H_0 = p_0 + \rho_0 v_0^2$ ranging from 0.1 to 10 dyn cm^{-2} and semilength L ranging from 10^8 to $5 \cdot 10^{10}$ cm, and with the shock position ranging from 1.24 to 1.95, in units of the loop semilength L. The models have the base temperature $T_0 = 2 \cdot 10^4$ K and zero heat flux at the base of the upflowing leg. As we have discussed in Paper I, the structure of the solutions does not change qualitatively and significantly if the heat flux ranges from 0 to

$-5 \cdot 10^3$ erg cm^{-2} s^{-1}. This insensitivity has been known since a long time and in a broader context than closed loop structures for instance it was explained in the solar wind context by Gonczi et al. (1977) and by Hammer (1982) in terms of a boundary layer theory.

As for the shocks in the descending critical solutions $y_>$, we have found that in any simulation the shock invariably leads to a solution of class 4 according to the definition of paper I, namely, an unphysical, double-valued solution which is not defined in all the loop but only at the beginning of the upflowing leg. Therefore, we have not studied shocked $y_>$ solutions any further.

4.1.1 Isothermal shocks

In the case of isothermal shocks the pre- and post-shock temperature are the same (the implicit assumption is that the thermal conduction is extremely high across the shock). Fig. 1 shows an example of the profile of the main physical quantities along a loop with $H_0 = 1$ dyn cm^{-2} and $L = 5 \cdot 10^{10}$ cm in the case of an isothermal shock (dashed line), and also in that of an adiabatic shock (solid line). We discuss the adiabatic shocks in Sect. 4.1.2.

For isothermal shocks, we have found that the larger is the base Mach number M_0 and the volumetric heating rate E_H, the lower is the shock position s_{sh}. As an example, in Fig. 2 we show s_{sh}/L vs. E_H and s_{sh}/L vs. M_0 for a loop with $H_0 = 1$ dyn cm^{-2} and $L = 5 \cdot 10^{10}$ cm for isothermal shocks (and also for adiabatic shocks, to be discussed in Sect. 4.1.2). All the cases shown in the figure, for both kinds of shocks, entirely cover the allowed range, as we have checked by trying to compute cases immediately adjacent to the limiting ones shown in figure and finding no solution. Similar tests have been done for all the following figures. In Fig. 2 we see that a change of 9% in E_H determines a change of $\sim 77\%$ in the position of the isothermal shock.

We have used the models computed with the numerical code to fit scaling laws relating the shock position and the characteristic parameters of the loop, finding

$$E_H = 7.5 \cdot 10^5 L^{-5/6} H_0^{7/6} \left(\frac{s_{sh}}{L}\right)^{0.1} \exp\left(-0.74 \frac{L}{s_p}\right) \tag{8}$$

$$M_0 = 1.35 (L H_0)^{-1/6} \left(\frac{s_{sh}}{L}\right)^{0.03} \exp\left(-0.8 \frac{L}{s_p}\right) \ , \tag{9}$$

where $s_p = 2 k_B T_{max} / \mu m_H g_0$ is the pressure scale height and T_{max} is the maximum temperature, with deviations not larger than 1.5% on 22 models with T_{max} ranging from $1.2 \cdot 10^6$ to $7.8 \cdot 10^7$ K, E_H ranging from $3.2 \cdot 10^{-4}$ to 0.37 erg cm^{-2} s^{-1} and M_0 ranging from 0.007 and 0.06. These laws are valid only for isothermal shocks in critical solutions.

4.1.2 Adiabatic shocks

Fig. 1 shows the distributions of the main physical quantities along the loop for a solution with an adiabatic shock. It is worth noting that, in this case, a jump in the temperature profile must be present, and recalling the RH condition on energy flow written as

$$\frac{T_+}{T_-} = \frac{2\gamma + (\gamma - 1) M_-^2}{2\gamma + (\gamma - 1) M_+^2} \ , \tag{10}$$

since $M_- > 1$ and $M_+ < 1$, invariably $T_+/T_- > 1$, i.e. the post-shock temperature T_+ is larger than the pre-shock temperature T_- and therefore the temperature profile has a local maximum after the shock.

For the adiabatic shock, we have found a different dependence of s_{sh}/L on E_H and M_0 with respect to the isothermal case. In all the cases that we have examined for the same volumetric heating rate there are two alternative positions of the adiabatic shock. As an example, Fig. 2 shows s_{sh}/L vs. E_H and s_{sh}/L vs. M_0 for a loop with $H_0 = 1$ dyn cm^{-2} and $L = 5 \cdot 10^{10}$ cm.

It is worth noting that more realistic and general shocks fall in between the two extreme cases considered by us, i.e. isothermal and adiabatic. As a consequence, the dependence of the shock position on the volumetric heating rate is, in the general case, intermediate between the two shown in figure. In Fig. 3 we compare the volumetric heating rates in adiabatic shocked solutions E_{ad} with the volumetric heating rates in isothermal shocked solutions E_{is}, computed according to Eq. (8), plotting s_{sh}/L vs. E_{ad}/E_{is} for three different loop semilength. It is worth noting that in the adiabatic case the volumetric heating rates are larger than in the isothermal case. In addition, a lower and an upper limit are present in the range of values of s/L over which an adiabatic shock can occur. The lower limit corresponds to the shock position with $M_{-}^{2} = 3$ (from Eq. (7)). The upper limit is dictated by the constraint that it cannot be arbitrarily close to the footpoint of the downflowing leg and, since the adiabatic shock leads to a significant upward jump of temperature, the temperature profile has to match the chromospheric boundary conditions of $2 \cdot 10^4$ K; the exact value of this upper bound, however, depends in a non-obvious way on L and E_H. Moreover, the figure shows that the range of s/L in which an adiabatic shock can form is closer to the loop apex in longer loops, and that longer loops have a larger range of volumetric heating rates.

Results analogous to those in Fig. 3 and obtained for a fixed loop semilength L have shown that E_{ad}/E_{is} does not change appreciably vs. the base dynamical pressure H_0 over a range between 0.1 and 10 dyn cm^{-2}, therefore we do not report them here.

4.2 Shocks in supersonic solutions

We assume, as before, that a shock connects the supersonic solution to a subsonic branch. This class of shocked solutions is characterized by supersonic velocity at the base of the upflowing leg which makes them, to some extent, peculiar. On the other hand, since the mass flux j is uniform along all the loop (cf. Eq. (1) and the RH conditions), the supersonic branch has lower mass density then the subsonic one due to its much larger velocity. As a consequence, supersonic flows should, generally, have low emission measure which would make them hardly observable. Although we do not claim that supersonic flows are frequent on the Sun, we suggest that loops with a shocked supersonic flow would be visible mostly (and, most likely, only) in the subsonic branch. This is in agreement with the observations that the line components characterizing supersonic flows are weaker, and then harder detected, than the subsonic line components as it is nicely discussed by Kjeldseth-Moe et al. (1993). From an observational point of view, we conjecture the possibility to see only a fraction of the loop in the solar atmosphere in these cases. Since these solutions are not unrealistic, we think that they can deserve more attention also from the observational point of view.

To produce the results discussed in the following two sections, we have analyzed a grid of coronal loops with base dynamical pressure ranging between 0.1 and 10 dyn cm^{-2}, semilength ranging between 10^8 and $5 \cdot 10^{10}$ cm, and base velocity ranging between $3.5 \cdot 10^7$ and 10^8 cm s^{-1} and with the shock coordinate ranging from 0.05 to 2, in units of L. The models have base temperature $T_0 = 2 \cdot 10^4$ K and heat flux at the base of the upflowing leg $F_0 = -10^3$ erg cm^{-2} s^{-1}.

4.2.1 Isothermal shocks

Fig. 4 shows the distributions of the main physical quantities of a loop in an isothermal shocked solution and in an adiabatic shocked solution, both with $H_0 = 1$ dyn cm^{-2} and $L = 10^9$ cm. We shall discuss the first case in this section and the second one in Sect. 4.2.2. In supersonic shocked solutions, the density values of the transition region in the supersonic branch can be several orders of magnitude smaller than in the subsonic branch, as shown in Fig. 4. As a consequence, the total emissivity in an optically thin, collisionally excited line of the transition region is several orders of magnitude smaller in the supersonic branch than in the subsonic ones, since it depends on the squared electronic density (see, e.g., Withbroe 1981), so that the lower region of the subsonic branch is much more visible than the corresponding region of the supersonic branch.

The exploration of this class of solutions has shown that, for given base dynamical pressure, loop semilength and base velocity, the shock position depends on the volumetric heating rate E_H of the loop, and there is a range of volumetric heating rates for which there are two alternative positions, depending on volumetric heating rate, where the shock can form. As an example, Fig. 5

shows s_{sh}/L vs. E_H/E_{law} (E_H is divided by E_{law}, the volumetric heating rate of the non-shocked supersonic solution computed with the scaling law (24) in appendix C, in order to facilitate the comparison of very different solutions), for solutions with three different values of base Mach number.

The analysis of many solutions like those shown in Fig. 5, and obtained for different values of M_0, H_0 and L (ranging respectively between 22 and 62, 0.1 and 10 dyn cm^{-2}, and 10^8 and $5 \cdot 10^{10}$ cm) shows that there exist two ranges of s/L where a shock leads to double-valued solutions of class 4, if the base velocity is low enough (but still supersonic). These solutions are not defined in all the loop but only at the beginning of the upflowing leg and they are not physically sound solutions of our problem. For instance, if we refer again to the example in Fig. 5, the case with $M_0 = 31$ and $M_0 = 62$ can shock anywhere, while in the other case (solid) the shock leads to unphysical solutions in the ranges $s/L < 0.5$ and $1 < s/L < 1.22$ (where we have not drawn the solid curve). Insight on this aspect comes from Fig. 6 where we show M^2 vs. s/L for some of these shocked solutions. In particular, we show that a shock occurring in a position $0.5 < s/L < 1$ and $s/L > 1.22$ (i.e. well within the existence range) leads the flow from the supersonic solution to a subsonic solution; the shock in $s/L = 0.5$ and $s/L = 1$, at the boundary of the region of existence, matches the supersonic solution with subsonic solutions very close to two *ascending* critical solutions $y_<$ but each with different boundary conditions, and similarly the shock in $s/L = 1.22$ (the lower boundary of the existence range) matches the supersonic solution, very close to the *descending* critical solution $y_>$, with a subsonic solution. Finally a shock for $s/L < 0.5$ or $1 < s/L < 1.22$ matches the supersonic solution with an unphysical solution. This shows how, for different shocks positions along the loop, we obtain different physical regimes and that the cases at the border of the regions where physically correct solutions exist are characterized by a transition to a solution very close to a critical solution. With an appropriate, finely tuned, choice of siphon flow parameters and boundary conditions we can obtain a solution which starts supersonic, undergoes a first shock leading to a critical solution which again shocks and finally reaches the chromospheric conditions at the end of the descending branch.

We have found the same dependence of E_H/E_{law} on s_{sh}/L for different values of H_0, L and M_0, ranging respectively from 1 to 10 dyn cm^{-2}, from 10^9 to $5 \cdot 10^{10}$ cm and from 22 to 62. As a consistency check, we note that, if $s_{sh}/L \sim 0$, the shock occurs at the beginning of the flow and our solution is virtually entirely subsonic; in this case, E_H, the volumetric heating rate required, is correctly described by the scaling law for subsonic solutions found in Paper I; on the other hand, if $s_{sh}/L \sim 2$, i.e. the shock is at the very end of the flow, $E_H = E_{law}$ in agreement with the solution being almost completely the supersonic solution.

4.2.2 Adiabatic shocks

We have explored the dependence of the adiabatic shock position on the volumetric heating rate for a range of values of H_0, L and M_0 (spanning respectively between 1 and 10 dyn cm^{-2}, 10^9 and $5 \cdot 10^{10}$ cm, and 22 and 62). In order to elucidate how the results on E_H depend on H_0, L and M_0, we show a few representative cases in Fig. 7. In each case there is a range of volumetric heating rates in which an adiabatic shock can occur and in most cases there are two alternative positions where the shock can form for the same volumetric heating rate. On the other hand, an adiabatic shock can occur only in a limited range of value of s/L; in fact, in Fig. 7, a shock in the ranges of s/L where we have not drawn data points would lead to unphysical solutions which are double-valued and not defined in all the loop; we have explored accurately the limits of the range as in the preceding figures. In each panel we show three s_{sh}/L vs. E_H/E_{law} profiles each for different M_0 values; the comparison of panel a) and b) shows how the profiles depend on H_0 and the comparison of panels a) and c) shows the effect of changing only L. All the panels of Fig. 7 show that increasing M_0 the range of s/L where a shock can occur is located closer to the upflowing footpoint, and the range of E_H/E_{law} values increases. The comparison between panels a) and b) shows that increasing H_0 leads to lower E_H/E_{law} values but this effect is not crucial. Comparing panels a) and c) we note that increasing L has a crucial effect which amounts to moving the boundaries (expressed in units of loop semilength) for the existence of shocked solution along the flow, and changing only slightly the curves shape.

5 Summary and conclusions

We have studied the physical conditions which allow the presence of either isothermal or adiabatic shocks both in critical and in supersonic siphon flow, i.e. all those cases having supersonic plasma velocities.

As for shocked *critical* solutions, the most important results of our analysis can be summarized as follows.

Both for the isothermal and for the adiabatic shocks, the shock position s_{sh} strongly depends both on the plasma volumetric heating rate E_H and on the base Mach number M_0, for fixed semilength L and base dynamical pressure H_0, but we have found different functional forms for the two kind of shocks.

The isothermal shock can occur everywhere in the supersonic branch of the critical solutions and E_H and M_0 depend monotonically on s_{sh}. For this class of shocks, we have derived scaling laws which relate the base dynamical pressure, the loop semilength, the volumetric heating rate, the base Mach number and the shock positions.

For the adiabatic shocks, E_H vs. s_{sh}/L is a bell shaped function, implying that the shock can occur in two different positions along the loop for the same E_H value and for the same boundary conditions at the base of the *upflowing* leg. It is worth noting that there is no real ambiguity on the choice of the shock position because it is determined by the boundary conditions at the base of the *downflowing* leg, for instance by the pressure value, which are different for the two shock positions. For the adiabatic shock there exists a limited range of E_H values, and correspondingly of M_0 values, over which a shock can form. Such a range corresponds to a quite limited range in the s/L domain and, for a given value of E_H, allowing a shock.

As for the shocked *supersonic* solutions, the position s_{sh} of both the isothermal and the adiabatic shocks depends on the volumetric heating rate E_H, for fixed L, H_0 and M_0. Again, the functional forms are very different in the two cases. For isothermal shocks, the profiles have an upward concavity, while for adiabatic shocks, it is bell shaped as for critical solutions.

In both cases we have explored the ranges of existence of shocks. For isothermal shocks, there exist ranges of s/L where a shock leads to unphysical solutions (namely, double-valued solutions which are not defined in all the loop) if the base velocity is low enough but still supersonic. For adiabatic shocks, the range of existence depends on M_0, H_0 and L: increasing M_0 it moves closer to the upflowing footpoint, increasing H_0 makes E_H/E_{law} lower, and increasing L moves the lower limit of the existence range upward along the loop.

We have also explored shocks in descending critical solutions $y_>$ and found that shocks in this class of solutions lead to unphysical solutions.

We have noted that the plasma in the supersonic branch of shocked siphon flows might be hardly detectable before the shock because the density is extremely low and radiative losses, depending on the square of density, would be negligible, with respect to the subsonic branch: only a fraction of the loop would be visible. The sudden increase of density and, in general, also of temperature immediately after the shock leads to an abrupt change of emissivity conditions which makes the shock in principle easily observable. Also critical shocked flows could be discriminated vs. the supersonic shocked flows because the first would have both loop feet clearly visible, while the second would show only the shocked subsonic branch.

This work has analyzed the set of shocked solutions possible in siphon flow. Analogously to Paper I, the focus has been almost entirely on the physical insight and on the exploration of the solution space in order to provide as clear a scenario as possible for further work.

In this respect, in future work, we plan to tackle the detailed prediction of emission from siphon flow loops including those subject to shocks. We will concentrate on the synthesis of loop emission in specific lines, and bands, also taking into account the non-equilibrium ionization, an effect known to influence the siphon flow line emission (e.g. Noci et al. 1989; Spadaro et al. 1990; Spadaro 1991; Peres, Spadaro and Noci 1992).

Acknowledgements. We wish to thank Dr. R. Hammer for his helpful comments. This work has been partially supported by Ministero della Università e della Ricerca Scientifica e Tecnologica and GNA-CNR.

A Derivation of equation (6)

The Rankine-Hugoniot conditions are

$$\rho_- v_- = \rho_+ v_+ \tag{11}$$

$$p_- + \rho_- v_-^2 = p_+ + \rho_+ v_+^2 \tag{12}$$

$$\frac{\gamma}{\gamma - 1}\frac{p_-}{\rho_-} + \frac{1}{2}v_-^2 = \frac{\gamma}{\gamma - 1}\frac{p_+}{\rho_+} + \frac{1}{2}v_+^2 , \tag{13}$$

where ρ is the mass density of plasma, v is the plasma velocity, and p is the pressure, and where we have marked with a minus sign the pre-shock quantities and with a plus sign the post-shock quantities. Eq. (11) and (12) lead to

$$c_+^2 = \frac{v_+}{v_-}(c_-^2 + v_-^2) - v_+^2 \tag{14}$$

where the isothermal sound velocity is defined as $c = \sqrt{p/\rho} = \sqrt{2k_BT/\mu m_H}$, with k_B the Boltzmann constant, $\mu = 1.257$ the mean atomic mass for solar abundances, and m_H the mass of the hydrogen atom. Eq. (13), with the definition of c_- and c_+ and substituting Eq. (14), leads to

$$\frac{\gamma}{\gamma - 1}c_-^2 + \frac{1}{2}v_-^2 = \frac{\gamma}{\gamma - 1}\frac{v_+}{v_-}(c_-^2 + v_-^2) + \left(\frac{1}{2} - \frac{\gamma}{\gamma - 1}\right) v_+^2 . \tag{15}$$

Solving for v_+, and excluding the trivial $v_+ = v_-$ solution, we obtain

$$v_+ = \frac{2\gamma}{\gamma + 1}\frac{c_-^2 + v_-^2}{v_-} - v_- \tag{16}$$

which, factorizing $v_-/(\gamma + 1)$, easily leads to Eq. (6).

B Derivation of inequality (7)

Taking into account the definition of the isothermal sound speed, the condition $v_+ < c_+$ leads to

$$\left(\frac{T_+}{T_-}\right)^{1/2} > \left(\frac{v_+}{v_-}\right) M_- . \tag{17}$$

The mass conservation RH conditions (Eq.(11)) can be written as

$$\frac{v_+}{v_-} = \frac{\rho_-}{\rho_+} = \frac{p_-}{p_+}\frac{c_+^2}{c_-^2} = \frac{T_+}{T_-}\frac{1 + M_+^2}{1 + M_-^2} . \tag{18}$$

Substituting M_+ from the equation

$$\frac{T_+}{T_-} = \left(\frac{M_-}{M_+}\right)^2 \left(\frac{v_+}{v_-}\right)^2 \tag{19}$$

into Eq. (18), we obtain

$$\frac{T_+}{T_-} = \frac{1 + M_-^2}{1 + M_-^2 (v_+/v_-)^2 (T_-/T_+)} \left(\frac{v_+}{v_-}\right) \tag{20}$$

which leads to

$$\frac{T_+}{T_-} = (1 + M_-^2) \left(\frac{v_+}{v_-}\right) - M_-^2 \left(\frac{v_+}{v_-}\right)^2 . \tag{21}$$

Eq. (21) and inequality (17) lead to

$$1 + M_-^2 > 2 \left(\frac{v_+}{v_-}\right) M_-^2 , \tag{22}$$

and, substituting v_+/v_- from Eq. (6) into Eq. (22), we obtain inequality (7).

C Scaling laws for supersonic solutions

In the present appendix we report scaling laws for supersonic solutions analogous to those reported in Paper I for subsonic flows.

In lack of any clue, we have assumed the functional forms

$$T_{max} = \nu (p_0 + \rho_0 v_0^2)^{\alpha'} L^{\alpha} \; \exp\left(\theta \frac{L}{s_p}\right) \tag{23}$$

$$E_H = \mu (p_0 + \rho_0 v_0^2)^{\gamma} L^{\delta} \; \exp\left(\omega \frac{L}{s_p}\right) \tag{24}$$

where T_{max} is the maximum temperature, E_H is the volumetric input power into the solar atmosphere, p is the pressure, ρ is the mass density of plasma, v is the plasma velocity, L is the semilength of the loop, and $s_p = 2k_B T_{max}/\mu m_H g_0$ is the pressure scale height. Such forms are analogous to those used in Paper I for subsonic solutions.

We have assumed that the coefficients ν, α, α', μ, γ, δ, θ and ω depend only on the base Mach number M_0, and, using the results of the numerical code for the grid of siphon flow loops models to fit the Eq. (23) and (24), we have derived the following coefficients

$$\nu = 2.6 \cdot 10^3 \frac{1}{\sqrt{M_0}} , \qquad \alpha' \equiv \alpha = \frac{3}{7} - \frac{1}{7}\frac{1}{\sqrt{M_0}} , \tag{25}$$

$$\theta = 0.05 - 1.8 \frac{1}{\sqrt{M_0}} , \qquad \mu = 2 \cdot 10^6 \frac{1}{M_0^2} , \tag{26}$$

$$\gamma = \frac{7}{5} - \frac{1}{5}\frac{1}{\sqrt{M_0}} , \qquad \delta = -\frac{1}{2} - \frac{2}{3}\frac{1}{\sqrt{M_0}} , \tag{27}$$

$$\omega = 0.05 - 3 \frac{1}{\sqrt{M_0}} . \tag{28}$$

where we have verified that the exponents of $(p_0 + \rho_0 v_0^2)$ and L in Eq. (23) are the same, i.e. $\alpha' = \alpha$. In the wide set of cases we have modelled, $\sqrt{M_0}$ ranges between 4.3 and 18, while the minimum value of the Mach number inside the siphon flows analyzed ranges between 1.1 and 80; therefore the scaling laws apply even to flows very close to the critical ones. With 80 models we have tested that the deviation for law (23) is 10% for T_{max} ranging from $3 \cdot 10^5$ to $1.2 \cdot 10^7$ K and 20% for law (24) for E_H ranging from 10^{-5} to 1.4 erg cm^{-3} s^{-1}.

At variance with the scaling laws for subsonic solutions, now the coefficients of the scaling laws depend inversely on the Mach number, and T_{max} and E_H tend to zero when $M_0 \to \infty$.

In Fig. 8 we show the maximum temperature (Eq. (23)) and the volumetric heating rate (Eq. (24)) for supersonic solutions vs. the base Mach number for base dynamical pressure $H_0 = 1$ dyn cm^{-2} and loop semilength $L = 4 \cdot 10^9$ cm. For the model corresponding to the minimum value of M_0 reported, the maximum Mach number is $= 1$. The horizontal lines correspond to the maximum temperature (solid) and volumetric heating rate (dashed) computed with the hydrostatic scaling laws (Serio et al. 1981). It is worth noting that the maximum temperature for supersonic solutions with large values of M_0 can be smaller than the maximum temperature for hydrostatic model.

References

Borrini G., Noci G., 1982, Solar Phys. 77, 153

Cargill P.J., Priest E.R., 1980, Solar Phys. 65, 251

Degenhardt D., Solanki S.K., Montesinos B., Thomas J.H., 1993, A&A 279, L29

Gonczi, G., Mangeney, A., Souffrin, P., 1977, A&A 54, 689

Hammer, R., 1982, ApJ 259, 767

Kjeldseth-Moe, O., Brynildsen, N., Brekke, P., Maltby, P., 1993, Solar Phys. 145, 257

Montesinos B., Thomas J.H., 1989, ApJ 337, 977

Noci G., 1981, Solar Phys. 69, 63

Noci G., Spadaro D., Zappalà R.A., Antiochos S.K., 1989, ApJ 338, 1131

Orlando, S., Peres, G., Serio, S., 1994, A&A, in press

Peres G., Spadaro D., Noci G., 1992, ApJ 389, 777

Press W.H., Flannery B.P., Teukolsky S.A., Vetterling W.T., 1986, Numerical Recipes. Cambridge University Press, Cambridge

Raymond J.C., Smith B.W., 1977, ApJS 35, 419

Robb T.D., Cally P.S., 1992, ApJ 397, 329

Rosner, R., Tucker, W.H., Vaiana, G.S., 1978, ApJ, 220, 643.

Serio, S., Peres, G., Vaiana, G.S., Golub, L., Rosner, R., 1981, ApJ, 243, 288.

Spadaro D., Zappalà R.A., Antiochos S.K., Lanzafame G., Noci G., 1990, ApJ 362, 370

Spadaro D., 1991, Adv. Space Res. 11, No. 1, 221

Spitzer L., 1962, Physics of fully ionized gases. Wiley, New York

Stoer J., Bulirsch R., 1980, Introduction to numerical analysis. Springer-Verlag, New York

Thomas J.H., 1988, ApJ 333, 407

Withbroe, G.L. 1981, in Activity and Outer Atmosphere of the Sun and Stars, ed. A.O. Benz, Y. Chmielewski, M.C.E. Huber, & H. Nussbaumer, (Sauverny: Observatoire de Geneve), P.1

Zel'dovich, & Y.B., Raizer, Y.P 1966, in Physics of Shock Waves and High-Temperature Hydrodynamic Phenomena, ed. Hayes, & Probstein (New York: Academic Press)

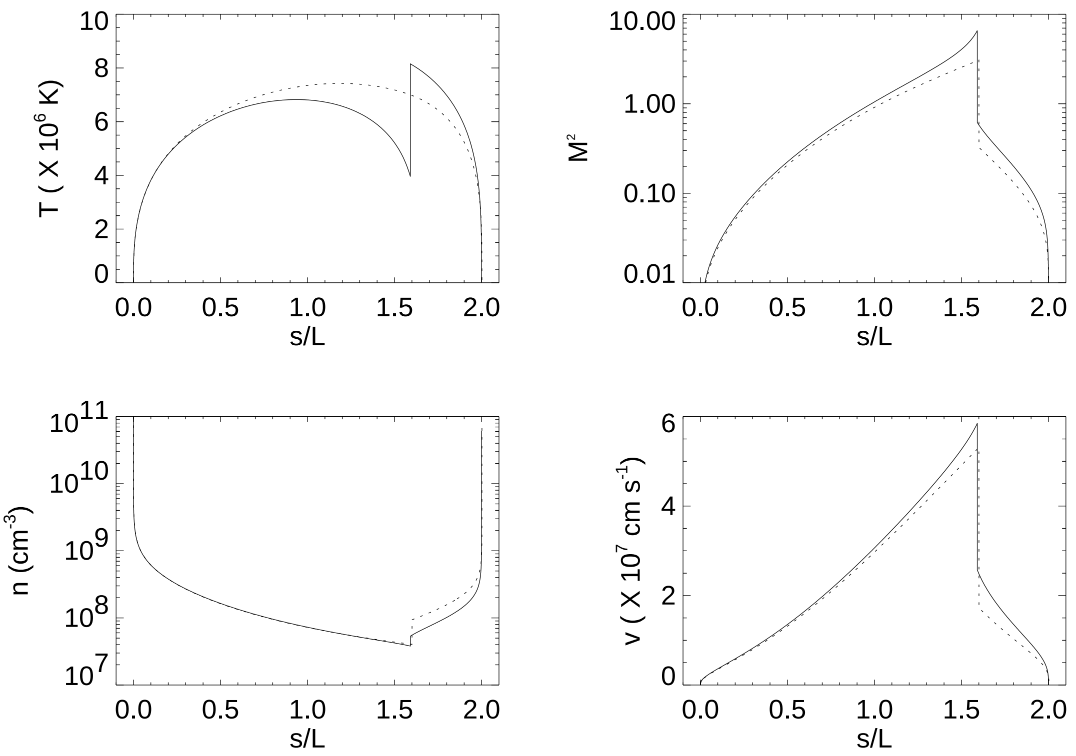

Figure 1: Profiles of temperature T, square Mach number M^2, electron density n and velocity v in a loop with $L = 5 \cdot 10^{10}$ cm and $H_0 = 1$ dyn cm^{-2}. The figure shows two critical solutions which have, respectively, an isothermal shock (dotted lines) and an adiabatic shock (solid line), both occurring at $s/L \sim 1.6$.

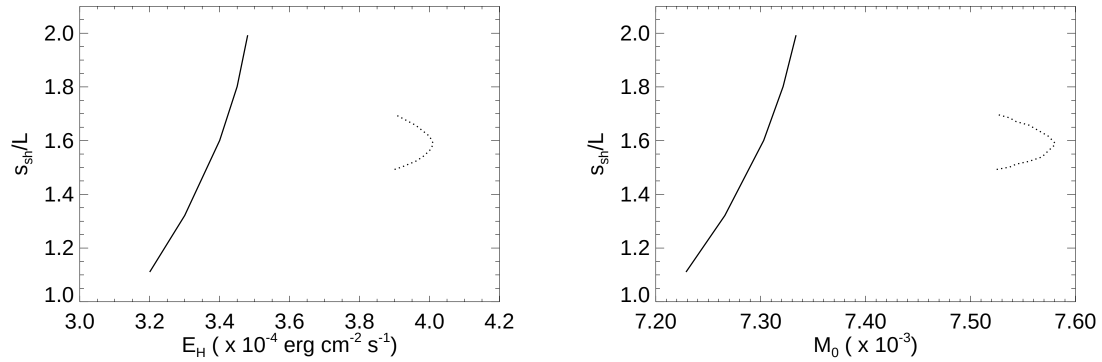

Figure 2: s_{sh}/L vs. E_H (panel on the left) and s_{sh}/L vs. M_0 (panel on the right) for a loop with $L = 5 \cdot 10^{10}$ cm, $H_0 = 1$ dyn cm^{-2} and $F_0 = 0$ for isothermal shocks (solid line) and for adiabatic shocks (dotted line), occurring in critical siphon flows.

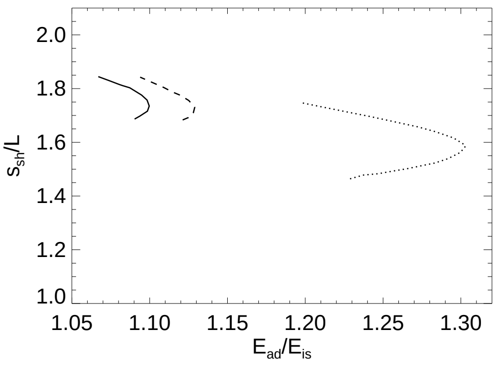

Figure 3: Normalized shock position, s_{sh}/L, vs. the ratio E_{ad}/E_{is} for a critical siphon flow loop with $H_0 = 1$ dyn cm^{-2} and three different semilength: $L = 10^8$ cm (solid), $L = 10^9$ cm (dashed), and $L = 5 \cdot 10^{10}$ cm (dotted).

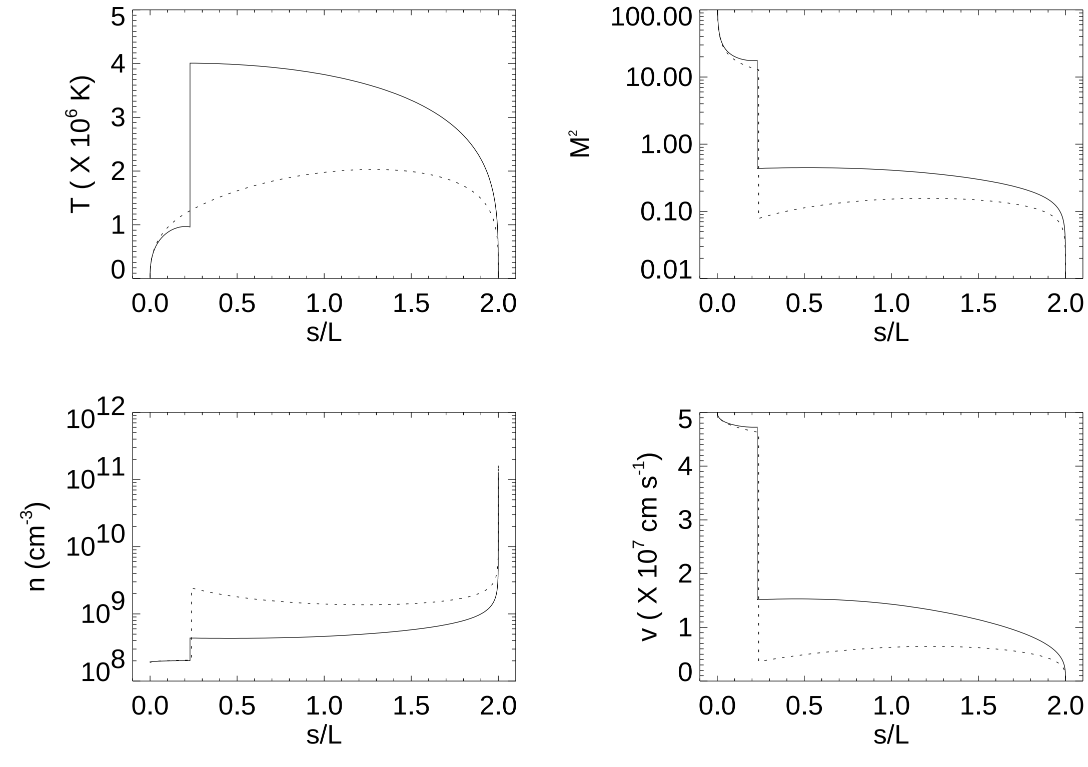

Figure 4: As in Fig. 1 for a supersonic siphon flow loop with $L = 10^9$ cm, $H_0 = 1$ dyn cm^{-2} and $v_0 = 5 \cdot 10^7$ cm s^{-1}. The figure shows two solutions with, respectively, an isothermal shock (dotted line) and an adiabatic shock (solid line), both occurring in $s/L \sim 0.22$.

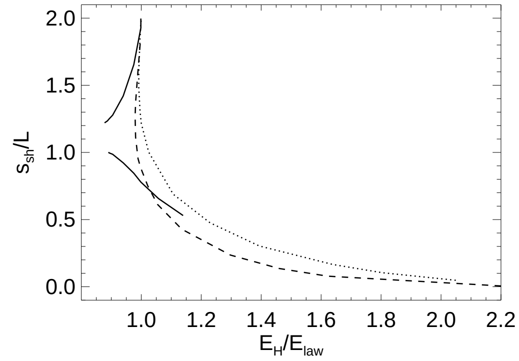

Figure 5: Normalized shock position, s_{sh}/L, vs. E_H/E_{law} for isothermal shocks occurring in supersonic siphon flow loop with $H_0 = 1$ dyn cm^{-2}, $L = 10^9$ cm and two different values of M_0, namely $M_0 = 22$ (solid), $M_0 = 31$ (dashed) and $M_0 = 62$ (dotted).

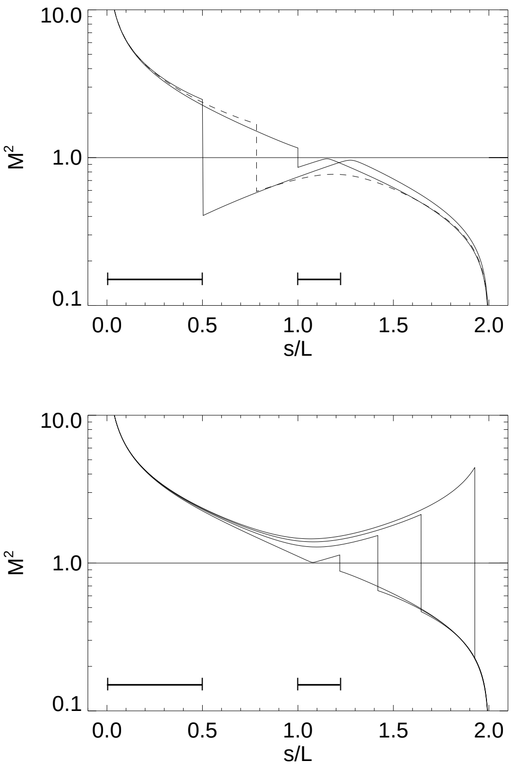

Figure 6: Square Mach number M^2 vs. s/L for supersonic shocked solutions with $H_0 = 1$ dyn cm^{-2}, $L = 10^9$ cm and $M_0 = 22$. In the upper panel we show solutions with a shock in the ascending branch and in the lower panel solutions with a shock in the descending branch. In both panels, we have marked the ranges of s/L where a shock cannot form.

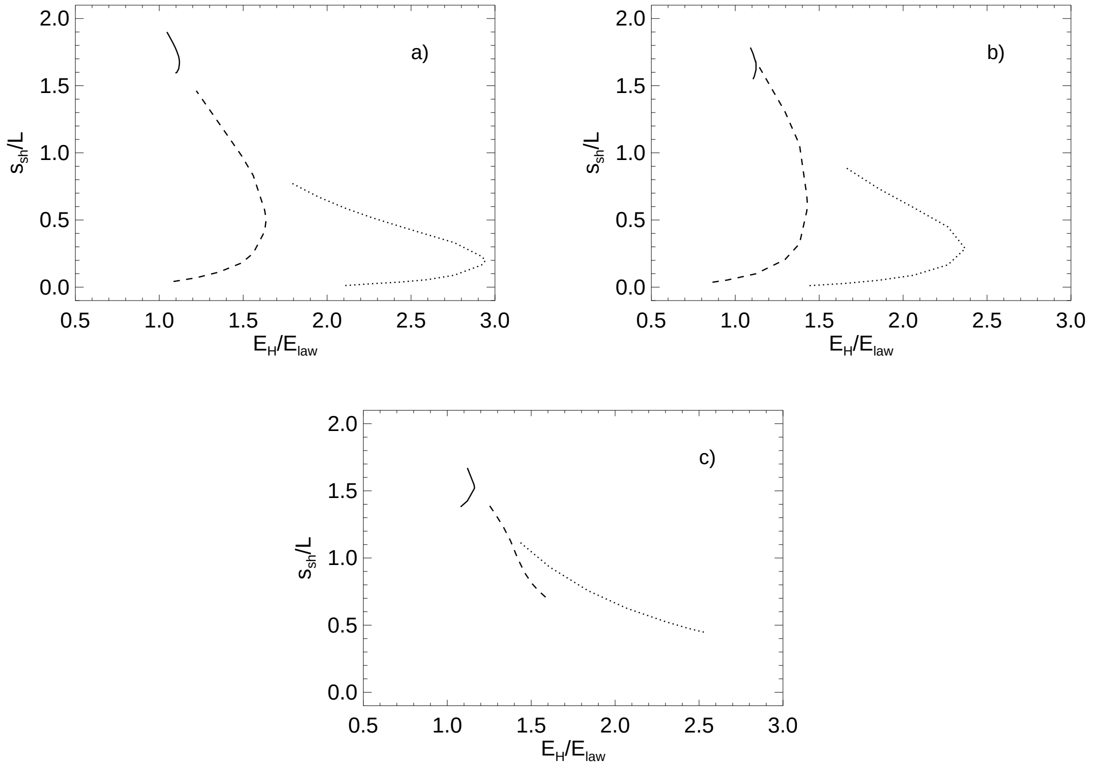

Figure 7: As in Fig. 5 for adiabatic shocks occurring in supersonic siphon flow loop with a) $H_0 = 1$ dyn cm^{-2}, $L = 10^9$ cm and $M_0 = 22$ (solid), 26 (dashed) and 31 (dotted), b) $H_0 = 10$ dyn cm^{-2}, $L = 10^9$ cm and $M_0 = 32$ (solid), 37 (dashed) and 43 (dotted), and c) $H_0 = 1$ dyn cm^{-2}, $L = 5 \cdot 10^{10}$ cm and $M_0 = 49$ (solid), 55 (dashed) and 62 (dotted).

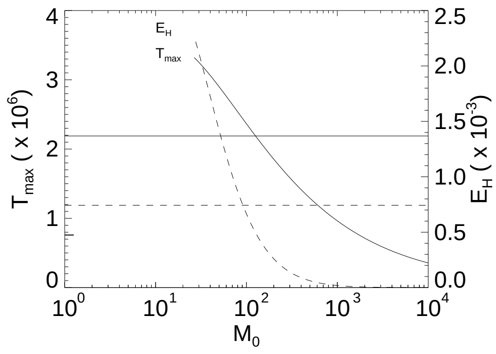

Figure 8: Maximum temperature T_{max} (solid) and volumetric heating rate E_H (dashed), respectively according to the scaling laws (23) and (24), vs. the base Mach number for a specific couple of L and H_0 values: $L = 4 \cdot 10^9$ cm and $H_0 = 1$ dyn cm^{-2}. The horizontal lines mark the maximum temperature (solid) and the volumetric heating rate (dashed) computed with the hydrostatic scaling laws. Since the scaling laws apply to supersonic solutions, the curves are drawn only up to the base Mach number M_0 corresponding to a minimum Mach number inside the loop equal to 1.